

Tailoring the magnetization reversal in antidot nanostructures using lithographically engineered inhomogeneities

D. Tripathy, P. Vavassori, and A. O. Adeyeye

Citation: *J. Appl. Phys.* **109**, 07B902 (2011); doi: 10.1063/1.3537948

View online: <http://dx.doi.org/10.1063/1.3537948>

View Table of Contents: <http://jap.aip.org/resource/1/JAPIAU/v109/i7>

Published by the [American Institute of Physics](#).

Additional information on J. Appl. Phys.

Journal Homepage: <http://jap.aip.org/>

Journal Information: http://jap.aip.org/about/about_the_journal

Top downloads: http://jap.aip.org/features/most_downloaded

Information for Authors: <http://jap.aip.org/authors>

ADVERTISEMENT



AIP Advances

Now Indexed in Thomson Reuters Databases

Explore AIP's open access journal:

- Rapid publication
- Article-level metrics
- Post-publication rating and commenting

Tailoring the magnetization reversal in antidot nanostructures using lithographically engineered inhomogeneities

D. Tripathy,^{1,a)} P. Vavassori,² and A. O. Adeyeye¹

¹Information Storage Materials Laboratory, Department of Electrical and Computer Engineering, National University of Singapore, Singapore 117576

²CIC nanoGUNE Consolider, 20018 Donostia-San Sebastian-IKERBASQUE, The Basque Foundation for Science, 48011 Bilbao, Spain

(Presented 18 November 2010; received 19 September 2010; accepted 2 November 2010; published online 17 March 2011)

We report on tailoring the magnetization reversal mechanism in engineered permalloy antidot nanostructures by lithographically introducing inhomogeneities in the form of neighboring antidots with alternate dimensions. We observed that the magnetic domain configurations are significantly altered when compared to homogeneous antidots due to the dissimilar size of adjacent antidots. The reversal process also is strongly influenced by the relative difference in the size of adjacent antidots and the thickness of the permalloy film. Our results have been further corroborated by micromagnetic simulations and low temperature measurements. © 2011 American Institute of Physics. [doi:10.1063/1.3537948]

There has been significant interest in the magnetization reversal mechanisms of patterned nanomagnets with precisely controlled geometry and interelement spacing due to potential applications in a wide range of magnetoelectronic devices such as magnetic random access memories,¹ read head sensors,² programmable logic devices,³ and ultrahigh density storage.⁴ From a fundamental viewpoint, nanomagnets by virtue of their low dimensionality offer a wide range of magnetic properties which are not observed in their continuous bulk counterparts, especially when the size becomes comparable to or smaller than certain characteristic length scales such as spin diffusion length, carrier mean free path, and magnetic domain wall width.⁵ One class of magnetic nanostructures that has received growing attention are antidots, which consist of arrays of “holes” embedded in a continuous magnetic film.⁶ The presence of “holes” can also modify the intrinsic magnetic anisotropy of the film, thereby inducing well defined periodic domain structures in the vicinity of the “holes.”⁷ With advancements in lithography tools for fabricating nanostructures with precisely controlled dimensions and geometry,⁸ it is now possible to create well defined antidot nanostructures with tailor-made physical parameters such as “hole” size and density⁹ and lattice geometry.¹⁰ The size and distribution of such engineered “holes” strongly affect magnetic properties such as coercivity, anisotropy, and reversal mechanism. Recently we have demonstrated that the use of two sublattices in bicomponent antidot nanostructures greatly enhances the parameters available for engineering the magnetic properties of antidots.¹¹

In this work, we investigate how the relative difference in the size of adjacent “holes” affects the magnetization reversal mechanism in antidot nanostructures as a function of temperature. We demonstrate that the reversal can be con-

veniently tuned by creating a differential in the dimensions of neighboring antidots.

A schematic of our proposed antidot nanostructure is shown in Fig. 1(a). Unlike homogeneous antidots, our structure is patterned such that there is a differential ($\Delta D = D_1 - D_2$) in the diameters of adjacent antidots. The experimental fabrication of such “inhomogeneous” antidots was achieved over a large area ($4 \times 4 \text{ mm}^2$) on commercially available Si substrates using deep ultraviolet (DUV) lithography at 248 nm exposing wavelength, followed by e-beam evaporation of permalloy ($\text{Ni}_{80}\text{Fe}_{20}$) films of varying thickness t and ultrasonic assisted lift-off in OK73 resist thinner. Details of the fabrication process are described elsewhere.⁸ Figure 1(b) shows the scanning electron microscope (SEM) image of two sets of “inhomogeneous” antidot nanostructures:

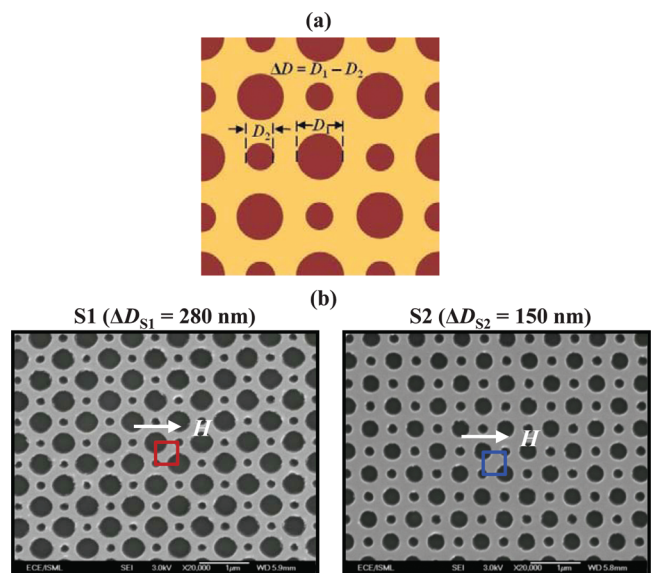


FIG. 1. (Color online) (a) Schematic illustration of the proposed antidot nanostructure with a differential $\Delta D = D_1 - D_2$ in the diameters of adjacent antidots. (b) SEM image of antidot nanostructures S1 and S2.

^{a)}Author to whom correspondence should be addressed. Electronic mail: eltdt@nus.edu.sg.

S1 with alternating diameters $D_1 = 450$ nm, $D_2 = 170$ nm, $\Delta D_{S1} = 280$ nm and center-to-center spacing between adjacent antidots fixed at $\lambda = 470$ nm; and **S2** with $D_1 = 350$ nm, $D_2 = 200$ nm, $\Delta D_{S2} = 150$ nm, and $\lambda = 450$ nm. For all the results shown in this work, the orientation of the external magnetic field H is along the edge of the square unit cell. Detailed insight into the magnetization reversal mechanism in the antidots was facilitated by micromagnetic modeling which was performed using LLG Micromagnetic software.¹²

Figure 2(a) shows the in-plane magnetization curves for antidot array **S1** at room temperature for $t = 30$ nm and $t = 80$ nm, respectively. The simulated magnetization curve for $t = 30$ nm is shown as an inset (i) in Fig. 2(a). Insets (ii) and (iii) show the respective half-loop derivatives of the magnetization curves. The corresponding anisotropic magnetoresistance (AMR) curves in the transverse geometry (field perpendicular to current density) are shown in Fig. 2(b). It is evident from both the magnetization and MR curves that in comparison to homogeneous circular antidot nanostructures of comparable dimensions and film composition,¹³ the magnetization reversal mechanism of our “inhomogeneous” antidot arrays is distinctly modified due to the alternating dimensions of adjacent antidots. The reversal occurs via two characteristic switching fields for both $t = 30$ nm and $t = 80$ nm, and also manifests itself in the two distinct peaks (G_1 and G_2) in the respective derivate loops. The simulated magnetization reversal for both **S1** and **S2** exhibits the same number of transitions [from A_1' to A_4' for **S1** as indicated in inset (i) of Fig. 2(a)] as observed in the experimental magnetization curves.

To better elucidate the reversal process, magnetization states obtained from LLG simulation at various stages of reversal are shown in Fig. 2(c) for $t = 30$ nm. At positive saturation field, all spins are aligned along the field direction. As the external magnetic field is reduced from saturation, domains form via demagnetizing fields due to surface magnetic charges at the boundary between the permalloy film and the antidot edges. Magnetization state A_1 in Fig. 2(c) shows that unlike homogeneous antidots where four wedge shaped domains connect each antidot to its nearest neighbor at each end,¹⁴ the domain patterns for our “inhomogeneous” antidots are altered. We observed that the wedge shaped domains now connect only the larger antidots ($D = 450$ nm) to their respective closest neighbors of identical dimension instead of the nearest neighbor smaller antidots ($D = 170$ nm), and the spins are oriented at $\pm 45^\circ$ to the field direction. The nucleation of wedge shaped domains around the smaller antidots is barely discernible, and they are unable to stretch out and connect to their counterpart antidots. The domain configuration may be ascribed to the additional anisotropy that has been induced in the “inhomogeneous” antidot nanostructures by patterning neighboring antidots with alternate dimensions.¹¹

With further reduction in magnetic field, we observed that magnetization continues to decrease gradually until there is a drop of $\sim 18\%$ at $H = 30$ Oe. We attribute this behavior to the formation of the domain pattern shown in state A_2 . Compared to A_1 , it can be seen that some of the wedge shaped domains connecting larger antidots have

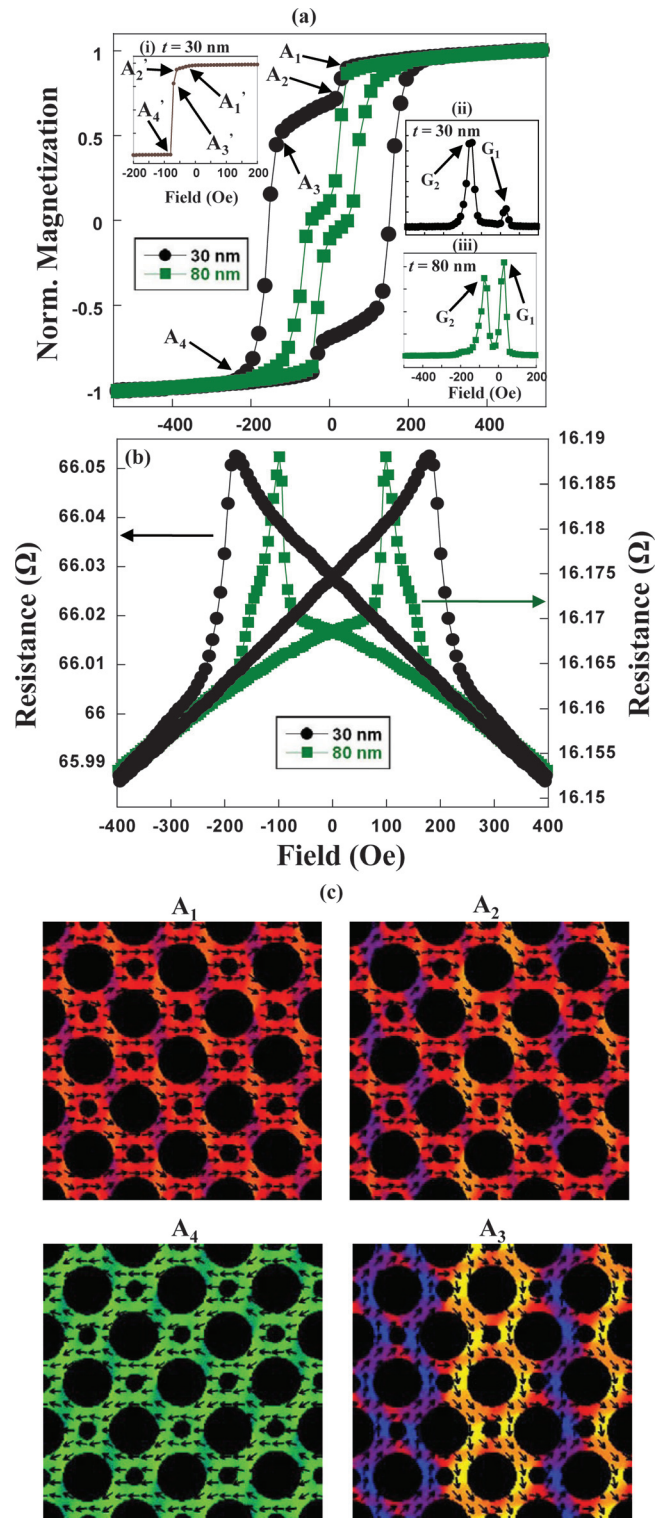


FIG. 2. (Color online) (a) In-plane magnetization curves with insets showing the simulated magnetization curve for $t = 30$ nm and the respective half loop derivatives. (b) Transverse MR cures for antidot array **S1** at room temperature. (c) Magnetization states obtained from LLG simulation at varying external magnetic fields for $t = 30$ nm.

increased in area, whereas others have concurrently decreased in area, thereby resulting in a reduction in the area of domains that are parallel to the applied field direction. This drop in magnetization is also accompanied by a change in slope of the MR curve in Fig. 2(b) due to further reduction

in the angle between magnetization and current density. When the field is now increased in the opposite direction, magnetization decreases continuously due to the rotation of domains until state A_3 is formed at $H = -150$ Oe. It can be seen that the wedge shaped domains from each of the smaller antidots have now coalesced with the adjacent larger domains, thereby resulting in a reduction in the area of domains that are parallel to the applied field direction. Furthermore we also observe that small vertical domains now exist between each pair of large/small antidots in every row of the structure and are oriented at $\pm 90^\circ$ to the field direction. We also note that for both A_2 and A_3 , the magnetization in the left side of the unit cell reverses slightly differently from the right side. This effect may be attributed to the fact that the SEM image was used to create the mask for the simulations, thereby taking into account the defect distribution at the edges of the “holes.” As the reverse field is increased further, a steep drop in both magnetization and resistance occurs and persists until the stable magnetic state shown as A_4 is formed at $H = -240$ Oe. A_4 represents the condition where all wedge shaped domains between the larger antidots have completed a 180° rotation from their original orientation in state A_1 , and the spins are now oriented at $\pm 135^\circ$ to the field direction. Further increase in reverse field signals the completion of magnetization reversal in the antidot nanostructures as all the spins align along the reverse field direction. For $t = 80$ nm, we observe a similar reversal mechanism with the first switching at $H = 30$ Oe. However, obvious distinctions were apparent in the considerably larger drop in magnetization ($\sim 75\%$) during the first switching, and the magnitude of the second switching field ($H = -75$ Oe). This may be attributed to the larger demagnetizing field as a consequence of increased film thickness.

Figure 3(a) shows the transverse MR curves for S_2 at room temperature for $t = 80$ nm. The difference in diameters (ΔD) of the neighboring antidots for S_2 is $\Delta D_{S_2} = 150$ nm, while for S_1 , the corresponding value is $\Delta D_{S_1} = 280$ nm. This suggests that for constant t , both structures should exhibit different switching mechanisms and magnetization states. We indeed observe that in sharp contrast to the reversal for S_1 (shown in Fig. 2), the reversal for S_2 occurs via three characteristic switching fields and is also evident clearly in the three peaks (H_1 , H_2 , and H_3) in the derivative loop (of the magnetization curve) shown as an inset in Fig. 3(a). This behavior has been attributed to the formation of transitional stable domain states in S_2 during the reversal process. While magnetization states similar to A_1 and A_4 also occur in S_2 , the difference in ΔD results in a different reversal mechanism with two intermediate magnetization states.

To eliminate the effects of thermally activated excitations on the reversal process at room temperature, we have also characterized the magnetic and transport properties of the antidot nanostructures as a function of temperature for $t = 80$ nm. We observed that the key features of the magnetization reversal process which were noticeable at room temperature also manifest themselves in the corresponding measurements at low temperature. The evident difference in the switching field distributions and the magnitudes of the characteristic

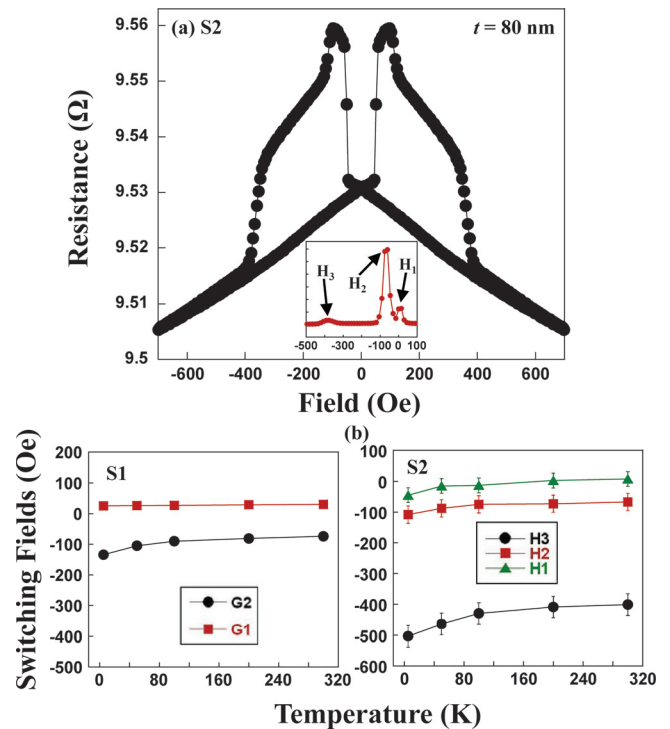


FIG. 3. (Color online) (a) Transverse MR curve with inset showing the half loop derivative for antidot array S_2 for $t = 80$ nm at room temperature. (b) Temperature dependence of switching fields for S_1 and S_2 corresponding to $t = 80$ nm.

switching fields (G_1 and G_2 for S_1) and (H_1 , H_2 , and H_3 for S_2) has been analyzed by extracting these fields from the half-loop derivatives of the magnetization curve and plotting them as a function of temperature in Fig. 3(b). All switching fields exhibit monotonic temperature dependence and increase noticeably in magnitude below 100 K.

This work was supported by the Agency of Science, Technology and Research (A*Star), Singapore, under Grant No. 062-101-0022 and National Research Foundation (NRF), Singapore, under Grant No. NRF-G-CRP 2007-05. P.V. acknowledges support from IKERBASQUE (the Basque Science Foundation), the Department of Industry, Trade, and Tourism of the Basque Government, the Provincial Council Gipuzkoa under the ETORTEK Program (Project No. IE06-172), and the Spanish MICINN (Project CSD2006-53).

¹G. A. Prinz, *Science*, **282**, 1660 (1998).

²M. Hehn *et al.*, *Science*, **272**, 1782 (1996).

³R. P. Cowburn and M. E. Welland, *Science*, **287**, 1466 (2000).

⁴R. L. White *et al.*, *IEEE Trans. Magn.*, **33**, 990 (1997).

⁵J. I. Martin *et al.*, *J. Magn. Magn. Mater.*, **256**, 449 (2003).

⁶A. O. Adeyeye *et al.*, *Appl. Phys. Lett.*, **70**, 3164 (1997).

⁷P. Vavassori *et al.*, *J. Appl. Phys.*, **91**, 7992 (2002).

⁸A. O. Adeyeye and N. Singh, *J. Phys. D: J. Phys.*, **41**, 153001 (2008).

⁹D. Tripathy *et al.*, *Appl. Phys. Lett.*, **93**, 022502 (2008).

¹⁰C. C. Wang *et al.*, *Nanotechnology*, **17**, 1629 (2006).

¹¹D. Tripathy *et al.*, *Appl. Phys. Lett.*, **97**, 042512 (2010).

¹²M. R. Scheinfein, LLG Micromagnetics Simulator (<http://llgmicro.home.mindspring.com>).

¹³C. C. Wang *et al.*, *Phys. Rev. B*, **72**, 174426 (2005).

¹⁴C. T. Yu *et al.*, *J. Appl. Phys.*, **87**, 6322 (2000).